JCTC Journal of Chemical Theory and Computation

United Atom Lipid Parameters for Combination with the Optimized Potentials for Liquid Simulations All-Atom Force Field

Jakob P. Ulmschneider*,† and Martin B. Ulmschneider‡

IWR, University of Heidelberg, Heidelberg, Germany, and Department of Chemistry, University of Utrecht, Utrecht, The Netherlands

Received February 19, 2009

Abstract: We have developed a new united-atom set of lipid force field parameters for dipalmitoylphosphatidylcholine (DPPC) lipid bilayers that can be combined with the all-atom optimized potentials for liquid simulations (OPLS-AA) protein force field. For this, all torsions have been refitted for a nonbonded 1−4 scale factor of 0.5, which is the standard in OPLS-AA. Improved van der Waals parameters have been obtained for the acyl lipid tails by matching simulation results of bulk pentadecane against recently improved experimental measurements. The charge set has been adjusted from previous lipid force fields to allow for an identical treatment of the alkoxy ester groups. This reduces the amount of parameters required for the model. Simulation of DPPC bilayers in the tension-free NPT ensemble at 50 °C gives the correct area per lipid of 62.9 ± 0.1 Å^2, which compares well with the recently refined experimental value of 63.0 Å^2. Electron density profiles and deuterium order parameters are similarly well reproduced. The new parameters will allow for improved simulation results in microsecond scale peptide partitioning simulations, which have proved problematic with prior parametrizations.

I. Introduction

In recent years computer simulations of proteins embedded in lipid bilayers have become a powerful tool to investigate this important class of proteins in its native environment. Advances in computer architecture now in principle allow classical all-atom molecular dynamics (MD) simulations of membrane proteins on the microsecond time scale, and much longer with coarse-grain models (see the recent review by Lindahl and Sansom).[1] This opens the possibility to directly observe the conformational transitions involved in protein function, such as gating and signaling. In addition, simulation time scales are now sufficient to study at atomic resolution the adsorption, folding, insertion, and self-assembly of many membrane-bound peptides, such as antimicrobials, viral channel formers, and synthetic peptides.[2−8] However, with the increased time scale of the simulations, there is a growing need to address deficiencies in the underlying models. At the time of their design most protein, water, and lipid force fields could not be tested beyond the picosecond to nanosecond range.[9] Especially tricky is the description of the membrane itself (i.e., the lipid force field) and the delicate balance of protein and lipid parameters. If such interactions are not well tuned, simulations can lead to results that are irreconcilable with experimental evidence and theoretical estimates: For example, in partitioning simulations of small hydrophobic peptides into lipid bilayers, unfolded conformations were buried in the hydrophobic core,[3] or were found to be favored over the expected transmembrane helix.[2,10] Such problems are most visible at slightly elevated temperatures where sampling is increased and for small peptides, where lipid−protein interactions dominate. For larger multispan membrane proteins, the protein−protein interactions are much stronger, making these problems difficult to detect at the time scales currently accessible. Indeed, because multiple helices are usually tightly locked through strong contacts of interdigitating hydrophobic side chains, it is in practice quite difficult to unfold membrane proteins in computer simulations. However, while the transmembrane

* Corresponding author e-mail: jakob@ulmschneider.com.
† University of Heidelberg.
‡ University of Utrecht.

10.1021/ct900086b CCC: $40.75
Published on Web 06/01/2009

part of the protein usually remains rigid, the subtle force field imbalances can manifest themselves in perturbations of the flexible parts such as extramembranous loop regions, leading to incorrect conclusions about the flexibility or function from simulation data.

Accurate and reliable lipid parameters are therefore of the utmost importance to derive meaningful data from computer simulations of membrane proteins. There are several lipid parameter sets in regular use for bilayer simulations, such as the all-atom (AA) CHARMM lipids,[11,12] including united-atom (UA) adaptations[13] and modifications.[14,15] Common UA models are the Berger[16] and GROMOS[17] lipid models. Other recent efforts have been based on the generalized AMBER force field[18,19] or polarizable models.[20] An excellent summary on the topic of lipid force field development has also been published recently.[21]

A troubling problem of several of these lipid force fields is the inability of simulated bilayers to sustain the fluid (L_α) phase area per lipid in the NPT ensemble. Instead, a dramatic lateral contraction is observed, either resulting in a bilayer that is too densely packed or even causing a transition into the ordered gel phase.[22] To compensate, a positive surface tension can be applied.[23] Finite size effects have been put forward as an explanation, yet other studies find only a small dependence of the area per lipid on the system size, especially if long-range electrostatic corrections are taken into account.[24] It seems the only significant finite size effect is on the lateral diffusion of the lipids, but not on structural properties.[25] Instead of a surface tension, another way to obtain the correct area per lipid is to simply fix the total box area to be constant (NPAT ensemble). Both the applied surface tension and NPAT simulations are problematic, since they require additional parameters. For each lipid type, lipid mixture, temperature, and embedded protein, a different value or the area or surface tension needs to be supplied, which is often not available. These parameters have also been shown to vary greatly with lipid type and hydration level.[26,27] In addition, simulations in the NPAT ensemble do not allow the membrane to stretch and breathe laterally, hindering important conformational transitions in membrane proteins or the insertion of peptides into membranes. Thus, such an approach is inappropriate for partitioning simulations. The delicate balance of large and opposing forces that goes into the lateral pressure profile indicates that a fragment-based parametrization strategy is possibly limited, and fitting to bulk lipid properties such as the area per lipid is required. Recently, Sonne et al. have described a reparametrization of the CHARMM force field to obtain greatly increased areas per lipid, though still 6% below experimental values for dipalmitoylphosphatidylcholine (DPPC).[14] Similarly, Högberg et al. have reported improved CHARMM parameters for tension-free simulations of dimyristoylphosphatidylcholine (DMPC).[15] Improved GROMOS parameters are also reported by Kukol.[28] Interestingly, even very recent new lipid parameter sets, such as the GAFF set,[19,29] or polarizable models,[20] do not provide the correct area per lipid in the tension-free NPT ensemble.

A lipid parameter set that yields reasonable areas per lipid in the NPT ensemble is the widely used UA model by Berger et al.[16] A UA description is beneficial for performance reasons: For example, an all-atom model of a DPPC molecule requires 130 atoms, while in UA models this number is reduced to 50. Thus, the calculation of lipid−lipid interactions is 6.7 times faster in the UA model. The Berger lipid paramters were essentially derived from previous united-atom optimized potentials for liquid simulations (OPLS-UA) studies by Essex et al.,[30] who described the first OPLS-UA lipid parameters by assembling parameters from studies of Jorgensen et al. on hydrocarbons,[31] ammonium ions,[32] and esters.[33] The missing types for connecting atoms between the various functional groups (choline, phosphate, glycerol) were obtained in an ad hoc fashion. For example, for C6 and C12 in DPPC, the methyls in dimethyl phosphate ($q = 0.2$, $\sigma = 3.8$ Å, $\varepsilon = 0.170$ kcal/mol) were adjusted to CH_2 united atoms by lowering the Lennard-Jones (LJ) well depth to $\varepsilon = 0.118$ kcal/mol, which is the value for a hydrocarbon CH_2 in OPLS-UA. Subsequently, Berger et al.[16] described a parameter set where the charges were replaced with entirely new values based on quantum mechanical calculations by Chiu et al.[23] The Berger set retained the LJ parameters of the Essex lipids, with the exception of the lipid tail hydrocarbon united atoms, which were refitted to reproduce thermodynamic data for liquid pentadecane. Torsions were assigned from GROMOS.[34,35]

Most commonly used simulation software cannot handle the simultaneous use of force fields that differ in their basic structure. Typically, LJ combining rules as well as 1−4 scaling factors for torsions are usually hard-coded and have to be unique throughout. This has made it difficult to perform simulations where the protein is modeled by OPLS-AA,[36] with a 1−4 scaling factor of 0.5, and the lipid parameters are modeled with the Berger set, which uses different torsions and scale factors. Some tricks have been proposed in the literature to overcome these problems, such as removing 1−4 interactions completely and refitting new torsions.[37] However, scale factors are critically important to describe both intra- and intermolecular interactions. Small or zero scale factors—where the complete 1−4 interaction is handled by the torsion potential—were found to be problematic.[36] Thus, it would be beneficial to have a set of lipid parameters with torsions refitted for a scale factor of 0.5 for both the LJ and Coulombic 1−4 interactions.

The present work has arisen from a desire for a simple UA lipid set that can be combined with the description of the protein using OPLS-AA. Starting from the Berger parameters, we report such a set. The major changes include a refitting of all torsions using quantum-mechanical profiles as the starting point, followed by further refinement in long time scale lipid bilayer simulations. In addition, the hydrocarbon lipid tail LJ parameters were reworked by long simulations of bulk liquid pentadecane. In the original study by Berger et al., a too low value of the heat of vaporization was used in the parametrization, resulting in lipid tail LJ interactions that are significantly too weak. Third, the charges on the major groups were adjusted to allow for a simpler parametrization in which the ester groups are treated equally. Finally, a key requirement of the new model was the

Table 1. Summary of Simulations of Pentadecane Performed in This Study[a]

		parameters							
		C2		C3					
	force field	σ (Å)	ε (kcal/mol)	σ (Å)	ε (kcal/mol)	time (ns)	thermostat	barostat	T (°C)
Gromacs	G96	3.96	0.091	3.96	0.136	20	Berendsen	Berendsen	25−50
Gromacs	OPLS	3.955	0.103	3.955	0.154	20	Berendsen	Berendsen	25
Hippo	OPLS	3.955	0.103	3.955	0.154	400	Andersen	MC	−20 to + 100

[a] All simulations were performed for 267 pentadecane molecules in a cubic box, with a nonbonded cutoff of 20 Å, long-range LJ cutoff corrections, and a time step of 1 fs, in the NPT ensemble at a pressure of 1 bar and the indicated temperature.

reproduction of the correct area per lipid in the NPT ensemble, without applying a surface tension.

II. Methods

All simulations were performed with the Hippo MD/Monte Carlo program (www.biowerkzeug.com) and Gromacs (version 4.0.2, www.gromacs.org).[38] The pentadecane simulations were run with 267 molecules in a cubic box in the NPT ensemble. In most of the MD simulations, the Andersen thermostat was used to maintain the temperature.[39] The pressure was kept constant at 1 bar by performing isotropic Monte Carlo pressure moves at intervals of 1000 time steps. Such moves involve the scaling of the box by a small random amount and a rejection/acceptance of the move using the Metropolis criterion.[40] Both the Andersen thermostat and Monte Carlo pressure moves have the advantage to suffer from no known artifacts, with the resulting statistics exactly representing the NPT ensemble.[40] Thus, we used these methods to obtain accurate numbers for the simulation parameters. In practice, the results are almost identical when other commonly known coupling methods are used, such as the Berendsen thermostat.[41]

The pentadecane simulations were run with Hippo using a simple nonbonded cutoff of 20 Å, with a smooth feathering to zero over the last 0.5 Å. Since there are no net charges on the aliphatic hydrocarbon united atoms, no Coulombic interactions need to be calculated, and no long-range electrostatic methods (e.g., particle-mesh Ewald (PME)) are necessary. For united-atom hydrocarbons, the electrostatic effects originating from the small polarizability need to be implicitly covered by the LJ terms. Long-range LJ interactions beyond the cutoff were included by using the usual correction terms.[40] This affects both the potential energy and—through the barostat—the system volume. Exact definitions of the cutoff correction are only available for homogeneous LJ fluids. If the system contains atom types with diverse LJ parameters, no exact description is possible, and the correction equation assumes a mix of the atomic parameters. The contribution of the cutoff correction to the energy scales with $\sim r_{\mathrm{cut}}^{-3}$. To avoid an unnecessary influence of the parametrization results on the details of the correction terms, a very large cutoff of 20 Å was chosen for the LJ interactions. This also minimizes potential differences due to the exact nature of the cutoff treatment, which is based on the distance of the center of charge groups. The time step was set to 1 fs to avoid the results being influenced by integrator errors. Simulations were 200 ns long, with the runs at 25 and 50 °C extended to 400 ns.

Control Monte Carlo simulations were also performed with Hippo using a setup identical to that of the MD runs. The results were similar to those of MD. Additional simulations of pentadecane were also performed with Gromacs using the Berendsen temperature and pressure coupling[41] and a cutoff of 20 Å. Finally, several simulations were performed with the original Berger hydrocarbon parameters.

For both pentadecane and DPPC, all bond and angle parameters were taken from previous studies.[16,30] Torsions were refitted for a 1−4 scale factor of 0.5 by matching against HF/6-31G* profiles obtained by dihedral scans on the usual lipid fragments, such as methyl acetate, glycerol, dimethyl phosphate, and choline, as described previously.[21] For the all-C2 torsion in the lipid tail, the more accurate MP2:CC data reported by Klauda et al. were used in the fitting, which results in a significant lowering of the *gauche* wells as compared to HF/6-31G*.[11] For example, in butane $\Delta E_{trans \rightarrow gauche} = 1.01$ kcal/mol for HF/6-31G*, but decreases to 0.63 kcal/mol for MP2:CC. Future improvement is possible by applying the higher theory also to the other dihedrals, but this is beyond the scope of the present study. Interestingly, dihedrals were not fitted previously for the Berger force field. In the orginal study, mainly standard torsions from the GROMOS force field were applied,[16] and a similar approach was used in a recent update of the Berger parameters by Kukol.[28] The lipid bilayer simulations were run in the NPT ensemble at 323 K, using weak temperature coupling with a coupling constant of 0.1 ps,[41] semi-isotropic weak pressure coupling, and no applied surface tension. Both systems with 50 and 128 DPPC molecules were studied. As the differences between the thermodynamic results were very small (see the Introduction), the results reported here are for the smaller system. Simulations were 100 ns long, with a time step of 2 fs. Bonds involving hydrogen atoms were constrained.[42] Water was represented using the TIP3P water model,[43] electrostatic interactions were treated by the PME method,[44] and LJ interactions used simple cutoffs ranging from 10 to 14 Å. The total sampling time reported in this work is ~3 μs, while the accumulated simulation time during the complete parametrization work was about ~15 μs.

III. Pentadecane Results

A. Pentadecane. The saturated lipid tails of DPPC are parametrized using pentadecane as the molecular fragment. Table 1 gives an overview of the simulation performed on pentadecane. A challenge in united-atom parametrization for liquid hydrocarbons is that all electrostatic effects (although minor, given their small polarizability) must be implicitly

Table 2. Density and Heat of Vaporization of Pentadecane for the Original Lipid Parameter Set

		ρ (g/cm^3)		ΔH_{vap} (kcal/mol)	
	r_{cut}[a] (Å)	25 °C	50 °C	25 °C	50 °C
Berger[b]	10		0.7457		14.77
Berger[c]	20	0.7584	0.7433	15.54	15.15
Chiu[d]	20	0.7788		18.40	
exptl[e]		0.7650	0.7478	17.41	16.96
exptl[f]				18.35	

[a] Cutoff corrections for long-range LJ interactions are included. [b] From ref 16 based on 10 ps simulations of pentadecane. [c] Based on 20 ns. [d] Reference 47. [e] Reference 45. [f] Reference 46.

incorporated through the LJ potential, whereas explicit charge dipoles can be used in all-atom descriptions. As the original saturated linear hydrocarbon OPLS-UA parameters were designed for smaller alkanes up to hexane,[31] Berger et al. obtained improved LJ parameters for pentadecane by fitting to the available liquid-phase experimental densities and heats of vaporization.[16] This was achieved by increasing the σ of both the C2 and C3 united atoms by 1.4% from 3.905 to 3.96 Å and greatly reducing ε by 23% from 0.118 to 0.091 kcal/mol for C2 and from 0.175 to 0.136 kcal/mol for C3. Combined with the proper torsion potential, these values result in a reasonable description of liquid pentadecane (see Table 2).

Since the original simulations at 50 °C were only 10 ps long, and used a rather small cutoff of 10 Å, but with LJ cutoff corrections, we performed several new pentadecane simulations with the same parameters, for 20 ns, and with a cutoff of 20 Å, including dispersion cutoff corrections. Despite the more thorough setup, we obtained almost similar results, with the density agreeing perfectly and ΔH_{vap} only

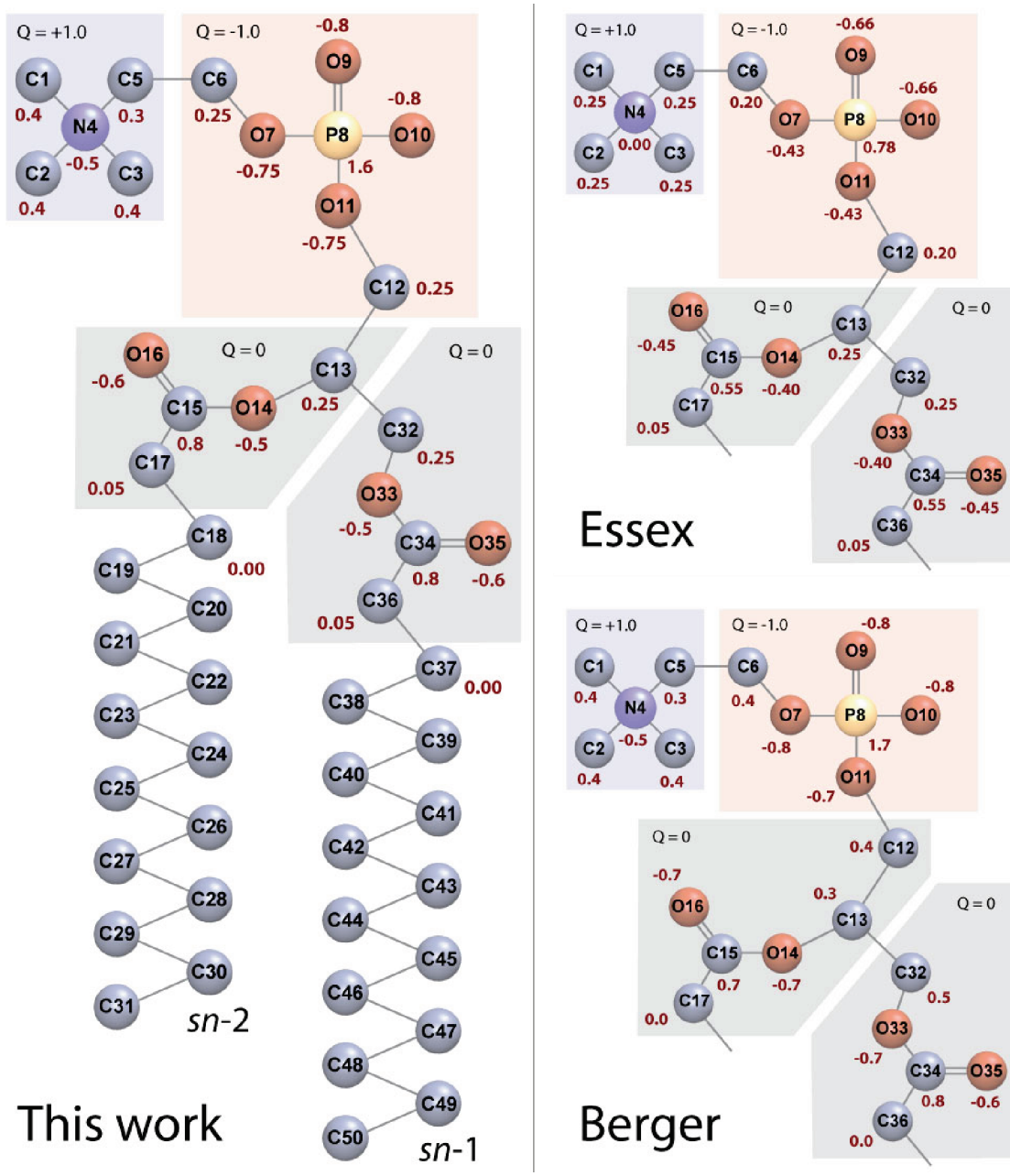

Figure 1. Illustration of a DPPC lipid molecule, with the charge groups and atomic charges indicated. Also shown are the values by Essex et al.[30] and Berger et al.[16]

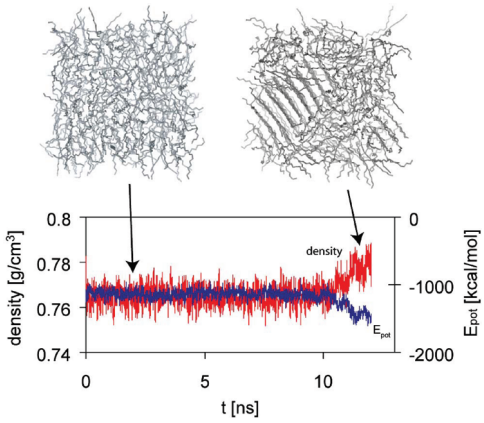

Figure 2. Example of a simulation of pentadecane that results in a freezing transition at ~11 ns.

slightly (2%) higher. This indicates that, for this almost homogeneous LJ fluid, the cutoff correction is very accurate, and it is not really necessary to use very high cutoffs of 20 Å. The density is also well matched against experimental data at both 25 and 50 °C. However, ΔH_{vap} seems to be underestimated by ~12% at both temperatures. The value of ΔH_{vap} is mainly dependent on ε, the strength of the LJ interaction. The low value of 15.5 kcal/mol reported by Berger et al. is due to the older experimental data used in that study.[16] More recent measurements indicate this value is substantially larger, ranging from 17.41 kcal/mol[45] to as high as 18.35 kcal/mol[46] at 25 °C (see Table 2). Subsequently, improved parameters for pentadecane with larger ε were reported by Chiu et al., resulting in $\Delta H_{vap} = 18.4$ kcal/mol.[47] The stronger LJ interactions will increase the attraction in the lipid tails and thus significantly affect the bilayer properties, such as lowering the area per lipid.[24] Thus, we chose to refit our new parameters to the higher values of ΔH_{vap} and over a larger temperature range.[45]

B. Melting Point Behavior. All equilibrium properties were obtained from a series of NPT simulations at temperatures ranging from 253 to 373 K. Below its melting temperature of 283.1 K, pentadecane freezes into stacked lamellae with regular hexagonal packing. Since the reproduction of liquid-state properties was the main goal here, all of the experimental values used in the fitting were from the liquid phase.

A poor parametrization of the hydrocarbon parameters can lead to freezing of the pentadecane box at temperatures above its melting point.[11] Figure 2 shows a simulation that spontaneously freezes due to incorrect parametrization, indicating that simulations should be in the multinanosecond range to detect such instabilities. Since the parameters are developed for the lipid tails, any incorrect parametrization with respect to the melting behavior will lead to bilayer simulations that show artificially high ordering, or even a gel phase. To determine the melting behavior of the present parameters, a series of simulations were performed at different temperatures to obtain T_{melt} for each parameter set. T_{melt} can only be calculated approximately due to the severe slowing of sampling near the phase transition, so there is an uncertainty of ±3 K, as illustrated in Figure 3. The melting point seems to be mainly affected by the energy difference

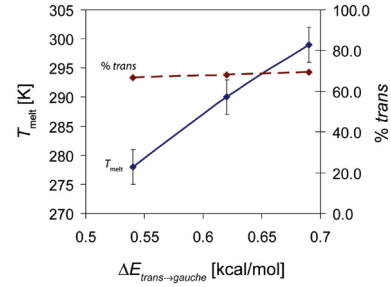

Figure 3. Dependence of the melting point T_{melt} of pentadecane on the conformational energy difference ΔE of the *trans* and *gauche* wells. An increase in ΔE of ~0.15 kcal/mol results in a positive melting point shift of ~21 K (solid line, left axis). The average population of *trans* states increases only slightly (dashed line, right axis).

Table 3. Results for the Simulations of Pentadecane[a]

	25 °C		50 °C	
	sim	exptl[b]	sim	exptl[b]
ρ (g/cm³)	0.7664	0.7650	0.7495	0.7478
ΔH_{vap} (kcal/mol)	17.46	17.41	16.88	16.96
κ (10^{-6} bar^{-1})	93.7	88.2[c]	111.8	104.1[d]
α (10^{-5} K^{-1})	88.4	89.1	92.3	93.1
C_p^{liq} (cal/(mol K))	107.5	112.3	112.2	115.3

[a] Density ρ, heat of vaporization ΔH_{vap}, isothermal compressibility κ, thermal expansion coefficient α, and liquid heat capacity C_p^{liq}. [b] Experimental data (except κ) from ref 45. [c] Reference 46. [d] Reference 72.

of the *gauche* and *trans* conformers $\Delta E_{trans \rightarrow gauche}$. By slight adjustments of the all-CH_2 torsion, a different melting point can be obtained without altering the thermodynamic properties too much. Figure 3 shows the dependence of the melting point on $\Delta E_{trans \rightarrow gauche}$. For a small increase in 0.15 kcal/mol, the melting point shifts upward by 21 K, while the average ratio of *trans* conformers of all rotatable bonds increases only minimally. These results indicate that torsional parameters must be carefully checked to accurately describe the liquid phase. Many previous lipid parametrization studies report sampling times too short to have detected such instabilities. In this study, we have verified that the melting point of both pentadecane and the DPPC bilayer is within 4 K of the experimental values.

C. Thermodynamic Properties of Pentadecane. Very good fits were obtained for the density, heat of vaporization, isothermal compressibility, thermal expansion coefficient, and constant-pressure heat capacity (Table 3). As a general trend, the density is mostly dependent on σ and the heat of vaporization on ε. We obtained the best fit for $\sigma = 3.955$ Å (C2 and C3) and $\varepsilon = 0.103$ kcal/mol (C2) and 0.154 kcal/mol (C3). This represents a lowering of the original OPLS values of ε by 12%, whereas in the Berger parametrization the reduction was 23%.[16] As a result, van der Waals interactions in the lipid tails are significantly stronger.

The density as a function of temperature is shown in Figure 4. The experimental data are represented as a solid line.[45] The standard deviations are very small due to the small fluctuation of the system box, and errors with respect to experiment are tiny, typically <0.5%. The heat of vaporization is obtained from $\Delta H_{vap} = \langle E_{gas} \rangle - \langle E_{liq} \rangle / N + RT$, where $\langle E_{gas} \rangle$ is the average potential energy of a single pentadecane

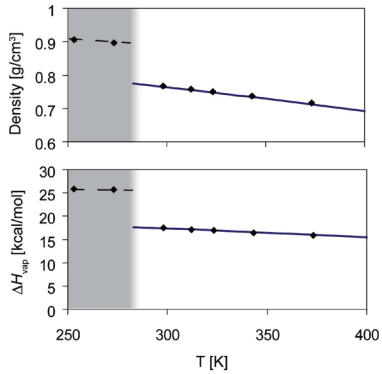

Figure 4. Density and heat of vaporization of pentadecane as a function of temperature. The results of the simulations are shown as dots. Experimental values for $T > T_{melt}$ are shown as smooth solid lines.[45] The shaded area represents the solid lamellar phase.

molecule in the gas phase (obtained from a Monte Carlo simulation) and $\langle E_{liq}\rangle/N$ is the average potential energy per molecule in the liquid phase. The agreement here is also almost perfect, and error estimates are very low since the potential energy of the system converges rapidly. Our value of $\Delta H_{vap} = 17.46$ kcal/mol at 25 °C matches the experimental one of 17.41 kcal/mol (c.f. Table 3). However, some experimental sources indicate this to be as high as 18.35 kcal/mol.[46]

While the density and ΔH_{vap} converge quite quickly, the remaining thermodynamic quantities are obtained from fluctuation formulas and require much longer time scales. To obtain fully converged results, the pentadecane simulations were extended to 400 ns each. The isothermal compressibility, κ, is computed from the volume fluctuations:

$$\kappa = \frac{\sigma_V^2}{\langle V\rangle kT}$$

where $\sigma_V = (\langle V^2\rangle - \langle V\rangle^2)^{1/2}$ is the standard deviation of the fluctuating system volume. A comparison of the calculated values versus experiment reveals that κ tends to be slightly overestimated, but the agreement nevertheless is very good (Figure 5). The thermal expansion coefficient α is given by

$$\alpha = \frac{\langle VH\rangle - \langle V\rangle\langle H\rangle}{\langle V\rangle kT^2}$$

where $H = E + PV$. Figure 5 shows the excellent correlation to the available experimental curve. Estimation of the liquid heat capacity C_p^{liq} is complicated by the improper classical description of vibrations in the fully flexible molecule. The standard procedure is to calculate only the fluctuations of the intermolecular enthalpy:

$$C_p^{inter} = \frac{\sigma_{H,inter}^2}{kT^2}$$

The full heat capacity for the liquid is then determined from $C_p^{liq} = C_p^{gas} + C_p^{inter}/N - R$, where C_p^{gas} is the experimental heat capacity for the ideal gas.[36] C_p seems to be slightly underestimated, although the agreement with experiment is still very good (Figure 5). The gas-phase contribution is quite large, typically 80%.

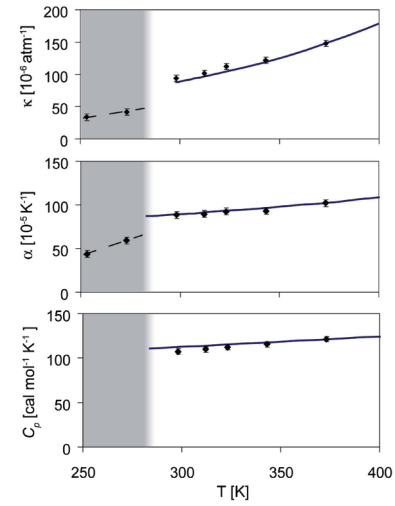

Figure 5. Isothermal compressibility κ, thermal expansion coefficient α, and liquid heat capacity C_p of pentadecane as a function of temperature. Experimental values for $T > T_{melt}$ are shown as smooth solid lines.[45,72] The shaded area represents the solid lamellar phase.

Despite the united-atom description, both the density and heat of vaporization can be reproduced with errors of <0.5% from experiment, while the other thermodynamic quantities are within ~5% of the experiments. Similar observations have been made with all-atom alkane force fields.[11,48] This also compares favorably to polarizable all-atom models for pentadecane, where the deviations from experiments were in fact slightly higher.[49] However, these parameters were designed to cover a wider range of hydrocarbons.

D. Role of the Thermostats and Barostats. The MD simulations were run with the Andersen thermostat and Monte Carlo volume moves to model the exact NPT ensemble (see the Methods). To compare to the more commonly used weak temperature and pressure coupling schemes, we repeated the simulations with these methods using Gromacs. The resulting density at 25 °C is $\rho = 7.670$ g/cm^3 (<0.07% difference), and $\Delta H_{vap} = 17.54$ kcal/mol (<0.4% difference). It seems that, for this system, the choice of the temperature and pressure coupling scheme has little to no influence on the equilibrium properties and that the values are reliable.

IV. Lipid Parameters

A. DPPC Parametrization. The next stage was the assembly of the new lipid parameter set. An illustration of a DPPC molecule is shown in Figure 1, together with the charges by Essex et al.[30] and Berger et al.[16] LJ parameters are the same on all atoms between these models, except the CH_2 and CH_3 groups in the lipid tails, which are based on the pentadecane simulations. One of the goals of the new parametrization was to have identical charges on both ester groups. This is the case in the Essex parametrization and in most other lipid force fields,[11,12,17] but not in the Berger set. Treating the ester groups similarly reduces the amount of fitting required substantially, leading to more robust and

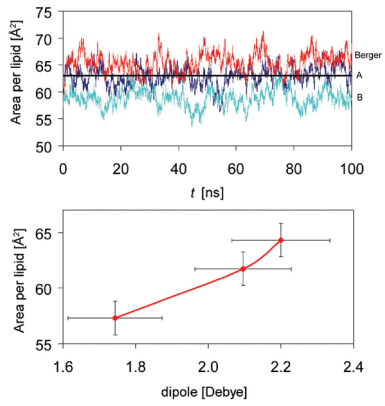

Figure 6. Upper panel: Area per lipid during the 100 ns simulations for the Berger parameters, this work (A), and a parameter set where only the charges in the headgroup were modified (B). The solid horizontal line represents the most recent experimental value of 63.0 Å^2.[51] Lower panel: Area per lipid dependence on the charge distribution of the ester groups by calculating the average ester dipole moment over all DPPC molecules over the complete simulation.

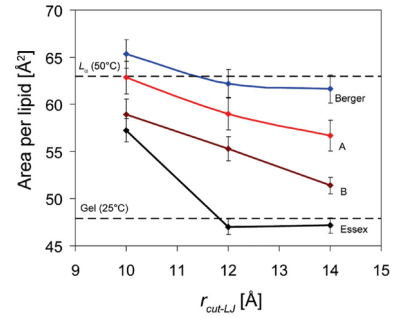

Figure 7. Dependence of the area per lipid on the van der Waals cutoff used in the simulations. Electrostatic interactions are evaluated using the PME method. The experimental values for the fluid (L_α) phase and gel phase are indicated as dashed lines.[26,51] There is a systematic decline of the area for all models as $r_{cut\text{-}LJ}$ is increased. The new model with more polar ester charges (A) results in higher areas than a model where only the headgroup is taken from the Berger set (B). The smallest decline is observed for the Berger set, due to the weak lipid tail LJ interactions. The Essex parameters show a transition into the gel phase.

transferable parameters. Although separate charge groups are no longer necessary when PME is used, it is beneficial to retain such groups to allow simple cutoff simulations. We thus started by slightly rearranging the charges of the Berger lipids to obtain the charge distribution illustrated in Figure 1. Further refinement was then based on reproducing experimental data in fully hydrated bilayer simulations.

The first test of the new parameters is whether simulated lipid bilayers retain the experimentally observed area per lipid A in the tension-free NPT ensemble. While experimental estimates of 57−71.2 Å^2 have been reported over the years (see the reviews by Nagle et al.),[26,50] we choose the more recent value of 63.0 ± 1.0 Å^2 obtained by simultaneously analyzing X-ray and neutron scattering data as the target of our parametrization.[51]

There is now a consensus that use of long-range electrostatic treatment (PME) is essential to obtain correct bilayer properties, while the use of a simple cutoff leads to bilayers that are too stretched and laterally shrunk.[52−54] This is easily understandable, given the strong charges in the lipid headgroups. Despite this, there remains a significant dependence of the area per lipid on the value of the LJ cutoff.[52] This is usually set to a low ∼10 Å for performance reasons. Given the nonisotropy of the bilayer environment, the use of simple analytic cutoff correction schemes that assume homogeneous isotropic liquids is problematic, although some advancements have been made in this direction.[55−57] The problem is acute for united-atom lipid molecules since the charges on the lipid tails are zero; i.e., there are only LJ interactions in the hydrophobic phase. With a small LJ cutoff, lipid tails interact at most with their first-shell neighbors. If the LJ cutoff is increased, the attractive nature of the LJ potential leads to more laterally compact bilayers.

The area strongly fluctuates (standard deviation of ±1.5 Å^2; see Figure 6) on the multinanosecond time scale, indicating that reliable numbers require simulations of at least 100 ns length. Figure 7 shows the obtained areas per lipid for various simulations as a function of the LJ cutoff. There is a systematic decline of ∼7−10% for all simulations as the LJ cutoff is increased from 10 to 14 Å. The lowest area is obtained for the Essex parameters, which results in an area of ∼57 Å^2, and a notably increased ordering of the lipid tails into parallel, mostly *trans* packing. For a larger cutoff, these parameters lead to a transition of the bilayer into the gel phase with the area shrinking to ∼47 Å^2. Bilayers simulated with the Berger set behave very differently. As previously observed the area is significantly larger at 65.3 Å^2,[54] and drops to only 60.9 Å^2 for the 14 Å LJ cutoff. This is a smaller decline than for the other models, and is caused by the weaker LJ interactions in the lipid tails of the Berger set. However, the much larger area is not due to the hydrocarbon parameters, but rather due to the differing charges on the polar part of the lipid molecule. The charge distribution on the headgroup developed by Chiu et al.[23] is much more polar than the values by Essex. Thus, we performed a series of bilayer simulations with the headgroup charges replaced by the Berger set, with some minor adjustments to achieve the charge group partitioning illustrated in Figure 1. Interestingly, the greatly modified phosphate and choline charges only lead to a marginal increase in the area to 58.9 Å^2 (Figures 6B and 7B). A similar insensitivity of the area per lipid on the headgroup charge distribution has been reported by Sonne et al.[14] This leaves only the ester groups (and glycerol) as the source for the higher area. As shown in Table 4, the original OPLS-UA parameters for esters are very similar to the more modern OPLS-AA ester charges obtained by Price et al.[58] In the Berger set, both the carbonyl and alkoxy O atoms are much more negative, and the carbonyl C is more positive. We therefore tried two new charge sets, one where the carbonyl C is made more positive but the oxygens are only slightly more negative (I), and one which is close to the Berger charges (II). The effect of these changes on bilayer properties is dramatic, with a strongly increased area per lipid of 62.3 Å^2 for set I and 62.9 Å^2 for set II (Figure 7A). This is very

Table 4. Electronic Net Charges on the Ester Group in Various Force Fields[a]

	O=	C	OS
OPLS-UA[b]	−0.45	0.55	−0.4
OPLS-AA[c]	−0.43	0.51	−0.33
Berger[d]	−0.7(−0.6)	0.7 (0.8)	−0.7
CHARMM for NPT[e]	−0.6	0.83	−0.47 (−0.54)
CHARMM for NPT (DMPC)[f]	−0.61	0.82	−0.54
this work (set I)	−0.55	0.7	−0.45
this work (set II)	−0.6	0.8	−0.5

[a] Charges in parentheses denote the second ester group. [b] Reference 31. [c] Reference 58. [d] Reference 16. [e] Reference 14. [f] Reference 15.

close to the recent estimate of 63.0 Å^2 by Kučerka et al.[51] Thus, we used these charges in our final parametrization.

The effect of the ester charges is also illustrated in Figure 6 (lower panel). There is a correlation between the dipole strength and the area per lipid, with the more polar ester group resulting in higher areas. We did not attempt a more thorough reparametrization of the ester charges beyond the goal of finding a charge set that is identical on both esters, but the results indicate that further investigation might bring additional improvements. Interestingly, the final charges on the esters are close to the values reported by Sonne et al. in their reparametrization of the CHARMM lipid force field (see Table 4), although the area per lipid reported in this study was significantly smaller (60.4 Å^2).[14] Almost identical charges are reported by Högberg et al., who obtained improved CHARMM parameters for DMPC.[15] Thus, it seems a general pattern that the ester charges should be more polar in lipid molecules to obtain correct bilayer properties, and are a major reason why the Berger parameters perform well. This is probably related to an increased hydration of the ester groups, but it could also be that the higher ester dipole simply covers for other imbalances in the lipid parameters. Further investigations will be performed in the future to clarify these observations.

B. Role of Headgroup Parameters. The phosphocholine headgroup of the lipid molecules exhibits a characteristic tilt toward the bilayer normal, which can be analyzed by calculating the distribution of the vector connecting the phosphorus and the nitrogen atoms, averaged over the course of the simulation and all lipid molecules. The resulting distributions for all parameter sets are shown in Figure 8. Despite the large differences in the partial charges of the phosphate and choline groups in the three models, the average orientation is perpendicular to the bilayer normal in all cases, with a tilt of ∼90°. The distribution is broad with $2\sigma = 60°$ in all cases. Similar values of 78−86° were found in previous studies with the Berger set,[19,59] and have been reported as low as ∼60° in other lipid force fields.[19] Overall, the parametrization changes in the headgroup seem to have little effect on the average headgroup orientation, which is interesting given the major differences between the Essex and Berger charges.

C. Order Parameter. The fine structure of the lipid bilayer and its ordering in the fluid phase can be measured experimentally using ^{2}H NMR spectroscopy. This involves deuterating hydrogens at selected carbon atoms and measuring the residual quadrupolar couplings of the CD bond. The

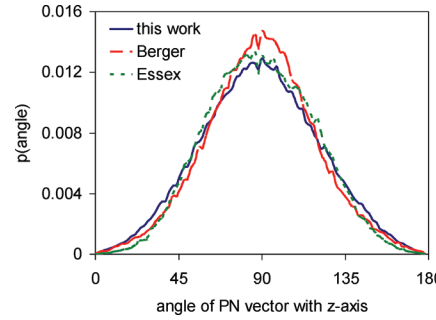

Figure 8. Distribution of the headgroup orientation vector (P−N) with respect to the bilayer normal for the individual models. The distributions are very similar, with the maximum at ∼90°.

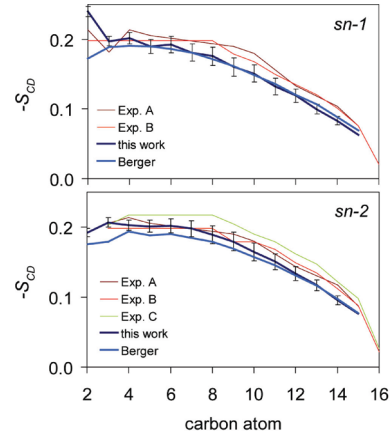

Figure 9. Deuterium order parameter for the two acyl chains of DPPC, for the simulations with the new parameter set (thick curve with error bars, estimated from block averaging), and the Berger lipids. Also shown are the experimental values of Seelig et al.[61] (A), Petrache et al.[62] (B), and Douliez et al.[63] (C).

resulting deuterium order parameter S_{CD} is a measure of the disorder and the relative orientation of the CD bond. S_{CD} is obtained from $S_{CD} = {}^2/_3 S_{xx} + {}^1/_3 S_{yy}$,[60] where the order parameter tensor is defined as

$$S_{\alpha\beta} = \frac{1}{2}\langle 3 \cos\theta_\alpha \cos\theta_\beta - \delta_{\alpha\beta}\rangle$$

with θ_α being the angle of the axis α (= x, y, z) to the bilayer normal (z axis) and the averaging taking place over molecules and time. In oriented samples, the axis of motional averaging is identical to the bilayer normal. Due to axial averaging, $S_{xx} = S_{yy}$ and $S_{xx} + S_{yy} + S_{zz} = 0$, resulting in[61]

$$S_{CD} = -S_{zz}/2 = \langle (3 \cos^2\theta_{CD} - 1)/2\rangle$$

Since no CD bonds are available on the united-atom carbons, either the deuteriums are constructed using ideal bond geometry or the vector from carbon C_{n-1} to C_{n+1} is used as the molecular axis for the nth CH_2 unit.[60]

Figure 9 shows the calculated S_{CD} parameters for both the *sn-1* and *sn-2* chains. The overall agreement with the experimental data is good.[61−63] S_{CD} values obtained for the Berger set are identical to those reported in a previous study by Patra et al.[52] The modified LJ parameters on the alkyl

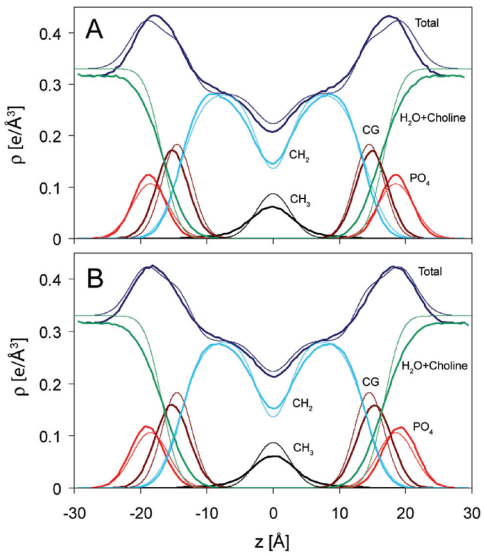

Figure 10. Electron density profiles from the simulations: (A) Berger lipids, (B) this work. The thick lines are the results of the simulations, averaged over the final 80 ns of the trajectory. The thin lines represent the experimental density determined by Kučerka and Nagle,[68] including the individual components (CG = carbonyl−glycerol).

chains will affect the torsional energetics and lipid ordering. Nevertheless, the changes are only small, with results for the *sn-1* chain similar to those of the Berger set and a slightly increased ordering in the *sn-2* chain. S_{CD} is strongly correlated to the area per lipid, with increased ordering for bilayers that are laterally too small. Values are also very sensitive to the *gauche* to *trans* energy difference of the alkyl torsions. Our results are in line with what has been reported previously on DPPC lipids.[11,14,52] A special case is the S_{CD} on C2. On the *sn-1* chain, this is in the high plateau region with $-S_{CD} = 0.215$, while it is split and much lower in the *sn-2* chain ($-S_{CD} = 0.15$ and 0.09).[61] With the new parameters, the S_{CD} on C2 is slightly higher than with the Berger parameters, which underestimates the S_{CD} on *sn-1*. On *sn-2*, both sets give a similar value that is too large compared to that from the experiments. Reproducing the splitting on *sn-2* would require abandoning the united-atom model and explicitly adding the CD bonds. Despite the absence of the deuteriums, the results show that S_{CD} can be accurately obtained even in the united-atom approximation.

D. Electron Density. The density distribution of the lipid bilayer can be measured by X-ray and neutron diffraction studies.[64] The total density is usually obtained from structure factors,[26,65,66] and the individual density contributions of the various lipid components can be extracted from structural models.[67] Computationally, the electron density is obtained by binning atoms along the direction of the membrane normal, weighted with the correct number of electrons, although it can also be calculated from the structure factors.[67] Figure 10 shows the electron density distribution of both the new model and the Berger set compared to the experimental results obtained by Kučerka and Nagle (H2 model).[68] There is a close agreement of the overall shape with the experimental data, with the characteristic headgroup peaks and the methyl troughs. As the water model underestimates the bulk

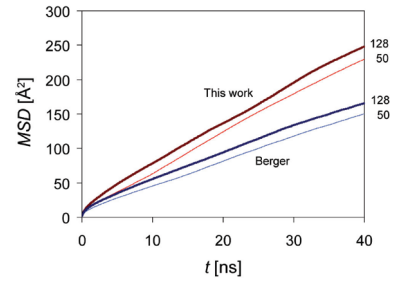

Figure 11. Average mean-square displacement of the lipid molecules as a function of time. Results for boxes containing 50 and 128 lipids are shown. The new parameters result in slightly faster lateral diffusion of the lipids, independent of the size of the simulated bilayer patch.

water density by 4% at 50 °C, the electron density differs by the same amount in the water phase. The experimental bilayer width (defined as the head-to-head distance) is 37.8 Å.[68] Our model gives a slightly smaller width of 36.6 Å, while the Berger set gives 35.6 Å. Individual components also compare well against the H2 hybrid model. Similar to what has been observed for the all-atom lipid CHARMM force field, there is an underestimation of the methyl peak in the bilayer center, which is compensated by an overestimation of the CH_2 density.[67]

E. Lateral Lipid Diffusion. Lipid bilayers are two-dimensional liquids characterized by the lateral diffusion of the individual lipid molecules. The lateral diffusion constant can be obtained from the Einstein relation

$$D_{lat} = \lim_{t\to\infty} \frac{1}{4t} \mathrm{MSD}(t)$$

where the mean-squared displacement is calculated as

$$\mathrm{MSD}(t) = \frac{1}{N}\sum_{i=1}^{N} \langle (\mathbf{r}_i(t + t_0) - \mathbf{r}_i(t_0))^2 \rangle$$

with $\mathbf{r}_i(t)$ is the position of the center of mass (CM) of lipid molecule i at time t, with averaging taking place over all time origins t_0. The results are shown in Figure 11. There is both a fast short-time diffusion caused by the fluctuation of lipid molecules in their trapped space and a slower long-time diffusion characterized by jumps of the lipid molecules from one basin to the next. Only the long-time diffusion is calculated here, by fitting the MSD over the linear phase from 20 to 30 ns. The resulting diffusion constants have to be corrected for the systematic CM motion of the two monolayers.[69] Klauda et al. have reported significant finite size effects in the lateral diffusion, with a ~3 times larger D_{lat} as the size of the lipid patch is decreased from 288 to 72 lipids.[25] To investigate a similar system size dependence, the simulations were performed with both 128 and 50 lipids. As can be seen from Figure 11, the lateral diffusion of both the new parameters and the Berger lipids depends only little on the system size, with a ~10% smaller D_{lat} for the 50-lipid systems in both cases. A slightly larger diffusion constant is found for the new parameters, with $D_{lat} = (16.5 \pm 0.9) \times 10^{-8}$ cm^2/s ($(15.3 \pm 0.8) \times 10^{-8}$ cm^2/s for 50 lipids), than for the Berger lipids, which have $D_{lat} = (11.4$

$\pm$ 0.8) $\times$ 10^{-8} cm^2/s ((10.0 $\pm$ 0.7) $\times$ 10^{-8} cm^2/s for 50 lipids). The new values closely match recent experimental estimates of $D_{lat} = 15.2 \times 10^{-8}$ cm^2/s (at 324 K) obtained from ^{1}H pulsed field gradient magic angle spinning NMR spectroscopy.[70] Earlier photobleaching experiments have reported $D_{lat} = 12.5 \times 10^{-8}$ cm^2/s at 323 K.[71] Thus, lateral diffusion is excellently reproduced by the new lipid parameters.

V. Conclusion

The new UA lipid parameters presented here have been designed to be used in combination with OPLS-AA for proteins. This avoids some of the tricks that have been necessary to use OPLS-AA in membrane protein simulations. A scale factor of 0.5 is now applied for all nonbonded 1−4 interactions throughout. In addition to refitting the torsion angles for the new scale factor, we have used the opportunity to improve on some of the other parameters of the Berger lipid force field: The acyl chains now have stronger LJ interactions, as determined from fitting to newer values of ΔH_{vap} of pentadecane. The stronger interactions do not lead to an incorrect freezing behavior, as special care was taken to ensure the melting points of both pentadecane and DPPC are not overestimated. In addition, the charge set of the Berger lipids is adjusted to allow symmetric carboxylate ester groups, simplifying the model and reducing the amount of torsions that have to be individually fitted. The area per lipid of 62.9 Å^2 is 3.5% lower than in the Berger force field, but exactly matches the more accurate recent experimental value of 63.0 Å^2 by Kučerka et al.[51] Electron density profiles and deuterium order parameters and lateral diffusion constants are also well reproduced. Most importantly, lipid bilayers can be simulated in the NPT ensemble without applying additional surface tension terms or having to fix the membrane surface area to be constant. Several recent lipid reparametrizatoin efforts have also focused on addressing this common lipid force field deficiency.[14,15] Tension-free NPT simulations are critical for studying peptide partitioning, where the membrane must be able to stretch laterally. The present work offers an accurate lipid parametrization for straightforward use with the widely employed OPLS-AA force field. The real test of the combined lipid and protein force field will be with multimicrosecond simulations of complex processes such as peptide adsorption, partitioning, and folding. To reach such time scales, the use of united-atom lipid molecules will remain crucial for the foreseeable future, given the vast computational advantage over all-atom lipids. This situation is similar to that of water molecules, where three-site models (SPC, TIP3P) are still used in the vast majority of simulations although more sophisticated, but slower alternatives exist. Additional work is currently under way to extend the present work to other classes of lipids and lipid mixtures.

Acknowledgment. This work was supported by BIOMS (J.P.U.) and the Human Frontier Science Program (M.B.U.). We thank Oliver Beckstein for helpful discussions and John F. Nagle for providing us with the experimental electron density curves.

References

(1) Lindahl, E.; Sansom, M. S. *Curr. Opin. Struct. Biol.* **2008**, *18* (4), 425.

(2) Ulmschneider, M. B.; Ulmschneider, J. P. *J. Chem. Theory Comput.* **2008**, *4* (11), 1807.

(3) Nymeyer, H.; Woolf, T. B.; Garcia, A. E. *Proteins* **2005**, *59* (4), 783.

(4) Ulmschneider, J. P.; Ulmschneider, M. B. *J. Chem. Theory Comput.* **2007**, *3*, 2335.

(5) Ulmschneider, M. B.; Ulmschneider, J. P. *Mol. Membr. Biol.* **2008**, *25* (3), 245.

(6) Ulmschneider, J. P.; Ulmschneider, M. B.; Di Nola, A. *Proteins* **2007**, *69*, 297.

(7) Im, W.; Brooks, C. L. *Proc. Natl. Acad. Sci. U.S.A.* **2005**, *102* (19), 6771.

(8) Im, W.; Brooks, C. L., III. *J. Mol. Biol.* **2004**, *337*, 513.

(9) Freddolino, P. L.; Liu, F.; Gruebele, M.; Schulten, K. *Biophys. J.* **2008**, *94* (10), L75.

(10) Ulmschneider, J. P.; Ulmschneider, M. B. *Proteins* **2009**, *75* (3), 586–597.

(11) Klauda, J. B.; Brooks, B. R.; MacKerell, A. D.; Venable, R. M.; Pastor, R. W. *J. Phys. Chem. B* **2005**, *109* (11), 5300.

(12) Feller, S. E.; MacKerell, A. D. *J. Phys. Chem. B* **2000**, *104* (31), 7510.

(13) Henin, J.; Shinoda, W.; Klein, M. L. *J. Phys. Chem. B* **2008**, *112* (23), 7008.

(14) Sonne, J.; Jensen, M. Ø.; Hansen, F. Y.; Hemmingsen, L.; Peters, G. H. *Biophys. J.* **2007**, *92* (12), 4157.

(15) Högberg, C.-J.; Alexei, M.; Nikitin, A. M.; Lyubartsev, A. P. *J. Comput. Chem.* **2008**, *29* (14), 2359.

(16) Berger, O.; Edholm, O.; Jahnig, F. *Biophys. J.* **1997**, *72*, 2002.

(17) Chandrasekhar, I.; Kastenholz, M.; Lins, R. D.; Oostenbrink, C.; Schuler, L. D.; Tieleman, D. P.; van Gunsteren, W. F. *Eur. Biophys. J.* **2003**, *32* (1), 67.

(18) Lula Rosso, I. R. G. *J. Comput. Chem.* **2008**, *29* (1), 24.

(19) Siu, S. W. I.; Vacha, R.; Jungwirth, P.; Bockmann, R. A. *J. Chem. Phys.* **2008**, *128* (12), 125103.

(20) Davis, J. E.; Rahaman, O.; Patel, S. *Biophys. J.* **2009**, *96* (2), 385.

(21) Feller, S. *Computational Modeling of Membrane Bilayers*; Academic Press: New York, 2008; Vol. 60.

(22) Feller, S. E.; Pastor, R. W. *J. Chem. Phys.* **1999**, *111* (3), 1281.

(23) Chiu, S. W.; Clark, M.; Balaji, V.; Subramaniam, S.; Scott, H. L.; Jakobsson, E. *Biophys. J.* **1995**, *69* (4), 1230.

(24) Wohlert, J.; Edholm, O. *Biophys. J.* **2004**, *87* (4), 2433.

(25) Klauda, J. B.; Brooks, B. R.; Pastor, R. W. *J. Chem. Phys.* **2006**, *125* (14), 144710.

(26) Nagle, J. F.; Tristram-Nagle, S. *Biochim. Biophys. Acta—Rev. Biomembr.* **2000**, *1469* (3), 159.

(27) Hristova, K.; White, S. H. *Biophys. J.* **1998**, *74* (5), 2419.

(28) Kukol, A. *J. Chem. Theory Comput.* **2009**, *5* (3), 615.

(29) Rosso, L.; Gould, I. R. *J. Comput. Chem.* **2008**, *29* (1), 24.

(30) Essex, J. W.; Hann, M. M.; Richards, W. G. *Philos. Trans. R. Soc. London, Ser. B* **1994**, *344* (1309), 239.

(31) Jorgensen, W. L.; Madura, J. D.; Swenson, C. J. *J. Am. Chem. Soc.* **1984**, *106* (22), 6638.

(32) Jorgensen, W. L.; Gao, J. *J. Phys. Chem.* **1986**, *90* (10), 2174.

(33) Briggs, J. M.; Nguyen, T. B.; Jorgensen, W. L. *J. Phys. Chem.* **1991**, *95* (8), 3315.

(34) van Gunsteren, W. F.; Krüger, P.; Billeter, S. R.; Mark, A. E.; Eising, A. A.; Scott, W. R. P.; Hüneberger, P. H.; Tironi, I. G. *Biomolecular Simulation: The GROMOS96 Manual and User Guide*; Biomos/Hochschulverlag AG an der ETH Zürich: Groningen, The Netherlands/Zürich, Switzerland, 1996.

(35) Egberts, E.; Marrink, S.-J.; Berendsen, H. J. C. *Eur. Biophys. J.* **1994**, *22* (6), 423.

(36) Jorgensen, W. L.; Maxwell, D. S.; Tirado-Rives, J. *J. Am. Chem. Soc.* **1996**, *118* (45), 11225.

(37) Tieleman, P.; Maccallum, J.; Ash, W.; Kandt, C.; Xu, Z.; Monticelli, L. *J. Phys.: Condens. Matter* **2006**, *18* (28), S1221.

(38) Hess, B.; Kutzner, C.; van der Spoel, D.; Lindahl, E. *J. Chem. Theory Comput.* **2008**, *4* (3), 435.

(39) Andersen, H. C. *J. Chem. Phys.* **1980**, *72* (4), 2384.

(40) Allen, M. P.; Tildesley, D. J. *Computer Simulation of Liquids*; Oxford University Press: Oxford, U.K., 1989.

(41) Berendsen, H. J. C.; Postma, J. P. M.; Vangunsteren, W. F.; Dinola, A.; Haak, J. R. *J. Chem. Phys.* **1984**, *81* (8), 3684.

(42) Hess, B.; Bekker, J.; Berendsen, H. J. C.; Fraaije, J. G. E. M. *J. Comput. Chem.* **1997**, *18*, 1463.

(43) Jorgensen, W. L.; Chandrasekhar, J.; Madura, J. D.; Impey, R. W.; Klein, M. L. *J. Chem. Phys.* **1983**, *79* (2), 926.

(44) Darden, T.; York, D.; Pedersen, L. *J. Chem. Phys.* **1993**, *98* (12), 10089.

(45) Yaws, C. L. *Chemical Properties Handbook*; McGraw-Hill: New York, 1999.

(46) Lide, D. R. *CRC Handbook of Chemistry and Physics*, 88th ed.; CRC Press: Boca Raton, FL, 2007.

(47) Chiu, S. W.; Vasudevan, S.; Jakobsson, E.; Mashl, R. J.; Scott, H. L. *Biophys. J.* **2003**, *85* (6), 3624.

(48) Thomas, L. L.; Christakis, T. J.; Jorgensen, W. L. *J. Phys. Chem. B* **2006**, *110* (42), 21198.

(49) Davis, J. E.; Warren, G. L.; Patel, S. *J. Phys. Chem. B* **2008**, *112* (28), 8298.

(50) Nagle, J. F.; Tristram-Nagle, S. *Curr. Opin. Struct. Biol.* **2000**, *10* (4), 474.

(51) Kučerka, N.; Nagle, J. F.; Sachs, J. N.; Feller, S. E.; Pencer, J.; Jackson, A.; Katsaras, J. *Biophys. J.* **2008**, *95* (5), 2356.

(52) Patra, M.; Karttunen, M.; Hyvonen, M. T.; Falck, E.; Lindqvist, P.; Vattulainen, I. *Biophys. J.* **2003**, *84* (6), 3636.

(53) Anezo, C.; de Vries, A. H.; Holtje, H.-D.; Tieleman, D. P.; Marrink, S.-J. *J. Phys. Chem. B* **2003**, *107* (35), 9424.

(54) Patra, M.; Karttunen, M.; Hyvonen, M. T.; Falck, E.; Vattulainen, I. *J. Phys. Chem. B* **2004**, *108* (14), 4485.

(55) Lagüe, P.; Pastor, R. W.; Brooks, B. R. *J. Phys. Chem. B* **2004**, *108* (1), 363.

(56) Shirts, M. R.; Mobley, D. L.; Chodera, J. D.; Pande, V. S. *J. Phys. Chem. B* **2007**, *111* (45), 13052.

(57) Klauda, J. B.; Wu, X.; Pastor, R. W.; Brooks, B. R. *J. Phys. Chem. B* **2007**, *111* (17), 4393.

(58) Price, M. L. P.; Ostrovsky, D.; Jorgensen, W. L. *J. Comput. Chem.* **2001**, *22* (13), 1340.

(59) Pandit, S. A.; Bostick, D.; Berkowitz, M. L. *Biophys. J.* **2003**, *84* (6), 3743.

(60) Egberts, E.; Berendsen, H. J. C. *J. Chem. Phys.* **1988**, *89* (6), 3718.

(61) Seelig, A.; Seelig, J. *Biochemistry* **1974**, *13* (23), 4839.

(62) Petrache, H. I.; Dodd, S. W.; Brown, M. F. *Biophys. J.* **2000**, *79* (6), 3172.

(63) Douliez, J. P.; Léonard, A.; Dufourc, E. J. *Biophys. J.* **1995**, *68* (5), 1727.

(64) Wiener, M. C.; White, S. H. *Biophys. J.* **1992**, *61* (2), 437.

(65) Benz, R. W.; Castro-Roman, F.; Tobias, D. J.; White, S. H. *Biophys. J.* **2005**, *88* (2), 805.

(66) Hub, J. S.; Salditt, T.; Rheinstädter, M. C.; de Groot, B. L. *Biophys. J.* **2007**, *93* (9), 3156.

(67) Klauda, J. B.; Kučerka, N.; Brooks, B. R.; Pastor, R. W.; Nagle, J. F. *Biophys. J.* **2006**, *90* (8), 2796.

(68) Kučerka, N.; Tristram-Nagle, S.; Nagle, J. F. *Biophys. J.* **2006**, *90* (11), L83.

(69) Lindahl, E.; Edholm, O. *J. Chem. Phys.* **2001**, *115* (10), 4938.

(70) Scheidt, H. A.; Huster, D.; Gawrisch, K. *Biophys. J.* **2005**, *89* (4), 2504.

(71) Vaz, W. L. C.; Clegg, R. M.; Hallmann, D. *Biochemistry* **1985**, *24* (3), 781.

(72) Dovnar, D. V.; Lebedinskii, Y. A.; Khasanshin, T. S.; Shchemelev, A. P. *High Temp.* **2001**, *39* (6), 835.

CT900086B